Computation of Three-Dimensional Viscous Flows Using a Space-Marching Method

K. N. S. Murthy* and B. Lakshminarayana†
The Pennsylvania State University, University Park, Pennsylvania

A space-marching method, developed to compute three-dimensional flows for internal geometries, has been utilized to predict viscous flows through a curved duct and over a swept wing. The Navier-Stokes equations have been posed as an initial value problem by neglecting the streamwise viscous diffusion terms and by treating the pressure gradient as a known source term. The resulting equations have been solved by a non-iterative (single pass) algorithm at each streamwise step. The results are compared with earlier computations (based on iterative methods) and the experimental data. The agreement between the present predictions, the experimental data, and the earlier predictions is good for the cases computed. The computation time is only a fraction of the iterative methods.

Nomenclature

c = chord length
c_p = pressure coefficient $2(P-P_\infty)$
$\hat{E},\hat{E}_s,\hat{E}_p,G,F,T,P,Q$ = vectors in governing equations, Eqs. (1) and (2)
e_i = specific internal energy normalized by U_∞^2
e = total fluxing energy normalized by $\rho_\infty U_\infty^2$
J = Jacobian of coordinate transformation
k = turbulent kinetic energy normalized by U_∞^2
L = characteristic length of the body or flow
M = Mach number
n = streamwise station index
p = static pressure normalized by $\rho_\infty U_\infty^2$
P_s = assumed static pressure
ΔP_{sc} = pressure correction, Eq. (6)
q = dependent flux vector
Re = Reynolds number of the flow based on characteristic length and velocity
r, θ, z = cylindrical coordinates normalized by a characteristic length
u, v, w = velocity components in z, θ, r direction normalized by U_∞. In the case of a curved duct, these are velocity components in x, y, z directions, respectively (see Fig. 1) normalized by bulk velocity
U = contravariant velocity component along ξ-direction ($\xi_z u + \xi_\theta v$)
x, y, z = local Cartesian coordinate for the curved duct (see Fig. 1) normalized by hydraulic diameter
γ = ratio of specific heats
ϵ = dissipation rate normalized by $U_\infty^3 L^{-1}$
μ = molecular viscosity normalized by μ_∞
ρ = density normalized by ρ_∞
τ = total shear stress normalized by $\rho_\infty U_\infty^2$
ξ, η, ζ = body-fitted coordinate system
$\xi_z, \xi_\theta, \eta_z, \eta_\theta, \xi_r$ = metrics of coordinate transformation
ω = vorticity/Rakich parameter (Eq. 4)

Subscripts

w = values on the wall
∞ = reference value
I = upstream value

Presented as Paper 84-1298 at the AIAA/SAE/ASME 20th Joint Propulsion Conference, Cincinnati, Ohio, June 11-13, 1984; received Aug. 18, 1984; revision received Dec. 11, 1984.

*Graduate Assistant, Department of Aerospace Engineering.
†Director of Computational Fluid Dynamics Studies and Professor of Aerospace Engineering, Department of Aerospace Studies. Fellow AIAA.

Introduction

MANY of the flows encountered in practice are three-dimensional and turbulent. Computation of such flows requires algorithms that incorporate the mean flow equations as well as adequate turbulence models. Of particular concern in this paper is flow through internal devices, such as turbomachinery rotors, ducts, cascades, diffusers, and inlets, where complex strain fields exist due to curvature, rotation, and pressure gradients.

The solution of the full Navier-Stokes equations by time-marching or relaxation schemes is prohibitively expensive and is rarely used in the design or analysis process on a day-to-day basis. One of the approximate but very efficient techniques is the so-called space- or parabolic-marching method. In this formulation a dominant flow direction is identified (e.g., primary flow direction in a curved duct or turbomachinery passage), and the viscous diffusion term in the streamwise direction is neglected. Patankar and Spalding[1] successfully developed an algorithm using this approximation with a bulk pressure correction. More vigorous schemes by Briley,[2] Ghia and Sokhey,[3] and Moore and Moore[4] have been successfully employed to predict complex flows. All these methods involve iterative methods for the solution of pressure using an additional equation. One of the drawbacks of these parabolic methods is the uncoupling of the governing equations and the use of an iterative scheme to couple them. In a flowfield with strong secondary flows and transverse velocity field, the convergence rate of such a scheme is slow.

In many situations, such as turbomachinery flows and flows in curved ducts, efficient inviscid solvers are available; hence, the inviscid pressure field can be accurately prescribed and the viscous correction to the pressure field can be accurately prescribed and the viscous correction to the pressure can be derived from a noniterative and efficient algorithm. Govindan[5] developed a space-marching method to compute three-dimensional viscous flows in internal geometries. The Navier-Stokes equations have been posed as an initial-value problem by neglecting the effects of streamwise diffusion and treating

the streamwise pressure gradient as a known source term. The fully coupled system of equations have been solved by a non-iterative algorithm at each streamwise step. A global pressure iteration can be used to capture the effects of the streamwise pressure gradient. The numerical scheme utilizes the strengths of previous methods and overcomes their weaknesses. The method incorporates some of the ideas developed by Schiff and Steger[6] in their marching procedures for the solution of steady supersonic viscous flows. The formulation is well posed mathematically and solvable. The governing equations have been written in a body-fitted coordinate system so that the method can be used to predict flows in complex geometries. A low Mach number formulation of the equations has been used to compute incompressible flow fields. The computer code based on this method has been used in this paper to predict three-dimensional viscous flows in a curved duct and over a swept wing.

Governing Equations and the Space-Marching Method

Details of the space-marching method and the computer code are given in Ref. 5. Only a brief description of the method will be given here. The Navier-Stokes equations in a cylindrical coordinate system (r, θ, z) are employed. This system is better suited for internal geometries and can be easily adopted to external flow configuration and the Cartesian system. To facilitate the application of boundary conditions, a body-fitted coordinate system is used. A grid transformation can be written as $\xi=\xi\ (z, \theta)$, $\eta=\eta\ (z, \theta)$, $\zeta=\zeta\ (r)$, where ξ is the coordinate in the marching direction and η is the coordinate approximately orthogonal to ξ on the cylindrical surface of radius ζ. ξ and ζ fit the boundaries along the boundary surfaces of the flow domain. The transformed equations can be written as

$$\frac{\partial \hat{E}(q)}{\partial \xi}+\frac{\partial \hat{F}(q)}{\partial \eta}+\frac{\partial \hat{G}(q)}{\partial \zeta}+\hat{C}(q)=\frac{1}{Re}\left[\frac{\partial \hat{T}(q)}{\partial \xi}+\frac{\partial \hat{P}(q)}{\partial \eta}+\frac{\partial \hat{Q}(q)}{\partial \zeta}+\hat{S}(q)\right] \tag{1}$$

where

$$q=[\rho, \rho u, \rho v, \rho w, \rho e_i]^T, \quad J\hat{E}=\xi_z E+\xi_\theta F$$

$$J\hat{F}=\eta_z E+\eta_\theta F, \quad J\hat{G}=\zeta_r G, \quad J\hat{C}=C, \quad J\hat{T}=\xi_z T+\xi_\theta P$$

$$J\hat{P}=\eta_z T+\eta_\theta P, \quad J\hat{Q}=\zeta_r Q, \quad J\hat{S}=S, \quad J=(\xi_z\eta_\theta-\xi_\theta\eta_z)\zeta_r$$

$\hat{E}$, $\hat{F}$, $\hat{G}$ contain the convective and pressure terms, $\hat{C}$ and $\hat{S}$ contain the curvature terms, and $\hat{T}$, $\hat{P}$, $\hat{Q}$ contain the viscous diffusion and the heat flux terms of the governing equations in cylindrical coordinates. Complete details on these vectors can be found in Ref. 5. Many of these vectors are standard and can be found in many references (e.g. Ref. 6).

For flows with a dominant flow direction, the Navier-Stokes equations can be parabolized by neglecting the streamwise diffusion terms ($\partial\hat{T}/\partial\zeta$). To make it a well-posed problem, dependence of the vector $\hat{E}$ on the pressure must be removed. The pressure terms are separated from the vector $\hat{E}$ to form a known source vector ($\hat{E}_p$) dependent on the assumed pressure field. Hence, the parabolized form of the Navier-Stokes equations can be written as

$$\frac{\partial \hat{E}_s(q)}{\partial \xi}+\hat{E}_p(p_s)+\frac{\partial \hat{F}(q)}{\partial \eta}+\frac{\partial \hat{G}(q)}{\partial \zeta}=\frac{1}{Re}\left[\frac{\partial \hat{P}(q)}{\partial \eta}+\frac{\partial \hat{Q}(q)}{\partial \zeta}+\bar{S}(q)\right] \tag{2}$$

where $\bar{S}(q)=\hat{S}(q)-Re\hat{C}(q)$. Equation (2) is a well-posed problem that governs the evolution of the flux vector $\hat{E}_s$. In the presence of strong pressure gradients, part of the streamwise pressure gradient in the momentum equation must be retained in E_s. Following Rakich,[7] Pouagare and Lakshminarayana[8] modified Govindan's formulation to derive the following expressions for $\hat{E}_s(q)$ and $\hat{E}_p(p_s)$:

$$J\hat{E}_s(q)=[\rho u, \rho uU+\xi_z(2\omega-1)p, \rho vU+\xi_\theta(2\omega-1)p, \rho wU, (e+p)U]^T \tag{3}$$

$$J\hat{E}_p(p_s)=(1-\omega)\frac{[p_s^{n+1}-p^{n-1}]}{\Delta\xi}[0, \xi_z, \xi_\theta, 0, 0]^T \tag{4}$$

where

$$\omega=\gamma M^2/[1+(\gamma-1)M^2]$$

The above form of $\hat{E}_s$ and $\hat{E}_p$ enables the algorithm to march through regions of strong streamwise pressure gradient (such as that which occurs near the leading edge of a wing or a cascade blade).

Numerical Technique

The numerical algorithm is based on the linearized block implicit scheme of Briley and McDonald[9] and Beam and Warming.[10] The difference scheme employed by Govindan[5] is given by

$$\left\{A-\frac{b_1\Delta\xi}{1+b_2}\left[\frac{\partial}{\partial\eta}\left(\frac{\partial B}{\partial q}\right)^n+\frac{\partial}{\partial\zeta}\left(\frac{\partial C}{\partial q}\right)^n\right]\right\}\Delta q^n=\frac{b_2}{1+b_2}\left(\frac{\partial \hat{E}_s}{\partial q}\right)^{n-1}\Delta q^{n-1}+\frac{b_1\Delta\xi}{1+b_2}(N^n-N^{n-1})+\frac{\Delta\xi}{1+b_2}\left[\frac{\partial B^n}{\partial\eta}+\frac{\partial C^n}{\partial\zeta}+S_I^n-N^n\right] \tag{5}$$

where

$$A=\left[\frac{\partial \hat{E}_s^n}{\partial q}-\frac{b_1\Delta\xi}{1+b_2}\left(\frac{\partial S_1}{\partial q}\right)\right]^n, \quad B=\left(\frac{\hat{P}}{Re}-\hat{F}+S_2\right)$$

$$C=\left(\frac{\hat{Q}}{Re}-\hat{G}+S_3\right), \quad N=\hat{E}_p$$

$$\bar{S}=S_1+\frac{\partial S_2}{\partial\eta}+\frac{\partial S_3}{\partial\zeta}, \quad \Delta q=q^{n+1}-q$$

It should be noted that the mixed derivatives in P and Q are treated explicitly and are not shown in Eq. (5).

Representing left hand side of Eq. (5) by R, and setting

$$-\frac{b_1}{1+b_2}\frac{\partial}{\partial\eta}\left(\frac{\partial B}{\partial q}\right)^n=L_\eta$$

$$-\frac{b_1}{1+b_2}\frac{\partial}{\partial\zeta}\left(\frac{\partial C}{\partial q}\right)^n=L_\zeta$$

Equation (5) can be simplified to

$$[A+\Delta\xi(L_\eta+L_\zeta)]\Delta q^n=R$$

Equation (6) can be factored based on the Douglas-Gunn split.

$$(A+\Delta\xi L_\eta)\Delta q^*=R$$

$$(A+\Delta\xi L_\zeta)\Delta q^{**}=A\Delta q^*$$

$$\Delta q^{n+1}=\Delta q^{**}$$

The parameters b_1 and b_2 determine the scheme employed. The results in the paper were obtained with $b_1=1$, $b_2=1/2$ corresponding to a three-point, backward implicit scheme with a truncation error of $0(\Delta\xi^3)$. In order to prevent uncoupling of odd and even points, a second-order artificial dissipation term was added to Eq. (5) on both the explicit and implicit sides.

This term has the form

$$\left[\frac{\sigma_i}{J}\frac{\partial^2\phi}{\partial\eta^2}+\frac{\sigma_i}{J}\frac{\partial^2\phi}{\partial\zeta^2}\right] \quad i=1 \text{ to } 5$$

where ϕ is ρ, $(\rho u, \rho u, \rho w)$ and e_i in the continuity, momentum,and energy equations, respectively. The artificial dissipation coefficients, $\sigma_i(i=1$ to 5) is chosen to be much smaller than the second order viscous terms. However, no damping terms were added in the case of the swept wing geometry.

Global Mass Flow, Pressure, and Velocity Corrections

In an internal flow computation, the specification of the global mass flow and the streamwise pressure gradient are mutually exclusive. In an internal flow computation where the global mass flow is specified and the streamwise pressure gradient approximated, requirements of uniqueness of the solution and the linearization errors in numerical scheme lead to a slow loss of the global mass flow. Maintenance of this constraint is important in internal flow computations and, therefore, the streamwise pressure gradient must be adjusted to prevent the loss of global mass flow. In the present algorithm this is done as follows:

1) After the solution is found at a particular streamwise station n, the change in the total mass flow is calculated, and the corrections to the streamwise pressure gradients and the velocity are derived from the following approximated formulas.

$$\Delta P_{sc}=-\Delta m/\int_\zeta\int_\eta \frac{\xi_z^2+\xi_\theta^2}{JU}\,d\zeta d\eta, \quad u_c=-\frac{\xi_z}{\rho U}\Delta P_{sc}$$

$$v_c=-\frac{\xi_\theta}{\rho U}\Delta P_{sc} \tag{6}$$

2) The pressure correction is used to correct the streamwise pressure gradient which is going to be used in the solution of the next streamwise station $n+1$.

3) The velocity corrections are used to correct the velocity at the current streamwise station n.

Turbulence Closure Models

The computation presented in this paper includes both the algebraic eddy viscosity and the k-ϵ models. The algebraic eddy viscosity model used is due to Baldwin and Lomax's.[11] It is a two-layer eddy viscosity model in which the eddy viscosity is calculated for an inner and an outer region. Algebraic eddy viscosity models, although simple to use, are found to be inadequate for three-dimensional flows. It is found that the the $k-\epsilon$ model of Jones and Launder[12] provides better predictions. This model has been incorporated in the code. Details of the equations used and the wall functions employed are given by Gorski et al.[13] and by Pouagare and Lakshminarayana.[8] The numerical procedure used lags the solution of the turbulence quantities (k and ϵ) by one streamwise step.

Initial and Boundary Conditions

The initial prescription of the pressure distribution is either assumed or computed using an inviscid code or is obtained from the experimental data. The initial velocity profiles are prescribed for the turning duct and are assumed to be uniform. For the swept wing, the measured pressure distribution is used. The present technique does not capture the elliptic effects. All the elliptic effects are included in the prescribed pressure distribution. The viscous correction to the pressure is derived from this algorithm.

The boundary conditions include no-slip on all the solid surfaces ($u=v=w=0$). Additional boundary conditions used in the spanwise direction for the swept wing are $\partial p/\partial\zeta=\partial\rho/\partial\zeta=\partial u/\partial\zeta=\partial v/\partial\zeta=\partial w/\partial\zeta=0$. This condition ensures uniformity in the spanwise direction. Experimental conditions were forced in the freestream.

Predictions and Comparison with Experimental Data

Curved Ducts[3,14]

The first case considered for study is a laminar flow in a curved duct of square cross section. The flow was measured by Mori et al.[14] and numerically investigated by Ghia and Sokhey[3] using a parabolic marching technique. The geometry of the duct is defined by the curvature ratio R/D, the aspect ratio A, and the total turning angle ϕ (Fig. 1). In the present case, R/D ratio of 14, aspect ratio A of 1.0, and turning angle ϕ of 103 deg were considered. The flow Reynolds number Re was 206 and the Dean number $K(=Re\sqrt{D/R})$ was 55. The flow developed under the presence of strong centrifugal force which tends to develop strong secondary flows resulting in cross flows perpendicular to the main flow direction.

The coordinate system used is shown in Fig. 1. The computation was carried out at a Mach number of 0.169, with 250 streamwise steps and a mesh size of 21×21 in the cross plane.

Development of the Streamwise Velocity

The development of streamwise velocity at the midsection AA is shown in Fig. 2. The streamwise velocity is normalized by the inlet velocity U_∞. It can be seen that the flow is almost symmetric and appears to be fully developed at $\theta=6.5$ deg. In the entry portion of the curved duct, the viscous forces tend to dominate over the centrifugal force. It is the centrifugal force

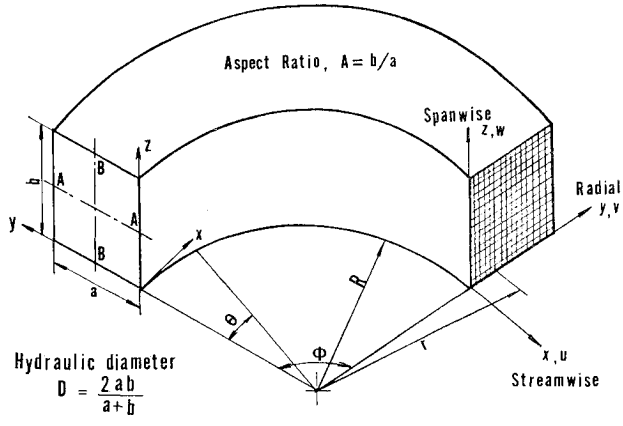

Fig. 1 Curved duct geometry and coordinate system.

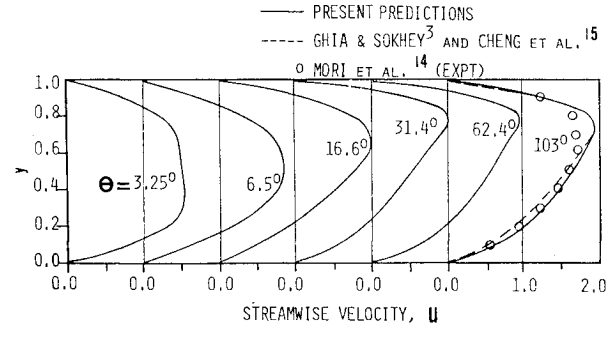

Fig. 2 Development of streamwise velocity profile along the midsection AA.

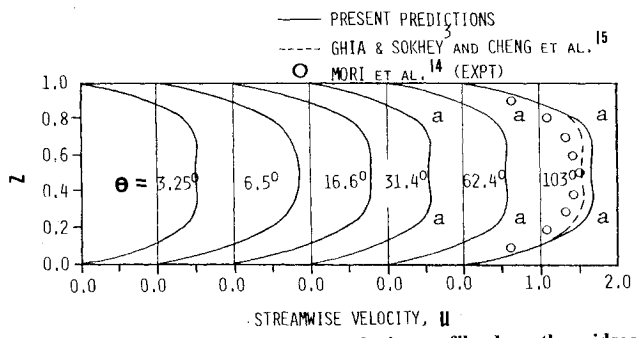

Fig. 3 Development of streamwise velocity profile along the midsection *BB*.

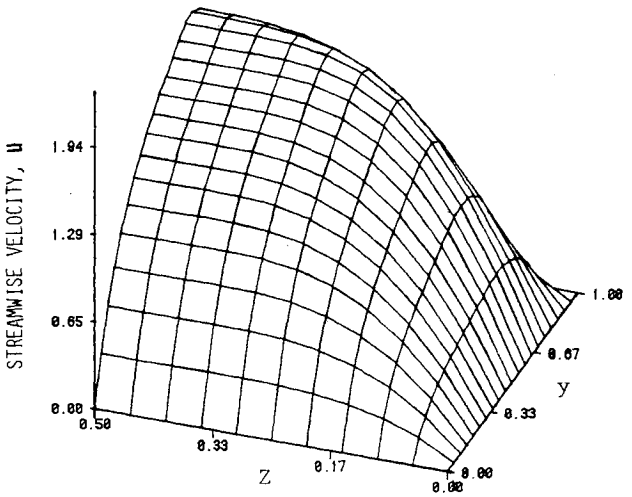

Fig. 4 Fully developed streamwise velocity at $\theta = 103$ deg.

that affects the symmetry and is negligible in the entry portion of the duct. The evolving flow in the streamwise direction is subjected to strong centrifugal forces, dominating over the viscous forces, the consequence of which is to cause the bulk of the flow to move toward the outer radius. This can be seen clearly in Fig. 2 for $\theta = 16.6$ deg to $\theta = 103$ deg. A peak velocity of 1.9 occurs at $y = 0.8$ when the flow is fully developed. The computed result at $\theta = 103$ deg is compared with the earlier numerical results of Ghia and Sokhey[3] and Cheng et al.[15] and experimental results of Mori et al.[14] The agreement with the results of Refs. 3 and 15 is good. However, there is a significant departure from the experimental results. This might have been caused by the differences in the mass flow rate. From Fig. 2 it appears that the experimental mass flow rate is lower than the mass flow used in the computation.

The development of the streamwise velocity at the midsection *BB* is shown in Fig. 3. The computed flowfield is symmetric about $Z = 0.5$ and exhibits two peaks, *aa*, as it evolves in the streamwise direction. This indicates the presence of two streamwise vortices of equal strength but of opposite sign. The predicted flowfield is in agreement with the numerical results of Ref. 3. The departure from the experimental data might be attributed to the reasons mentioned earlier. Figure 4 shows a three-dimensional plot of the computed, fully developed streamwise velocity.

Secondary Flow and Vorticity Development

The y variation of the spanwise velocity w at $z = 0.1$, 0.2, 0.3, and 0.4 for $\theta = 103$ deg is shown in Fig. 5. The v velocity distribution with respect to z at $y = 0.2$, 0.4, 0.6, and 0.8 for $\theta = 103$ deg is also shown in Fig. 5. It is clear that the two vortices of equal strength but of opposite sign are located at $y = 0.6$. The computed results are in good agreement with the numerical results of Ref. 3.

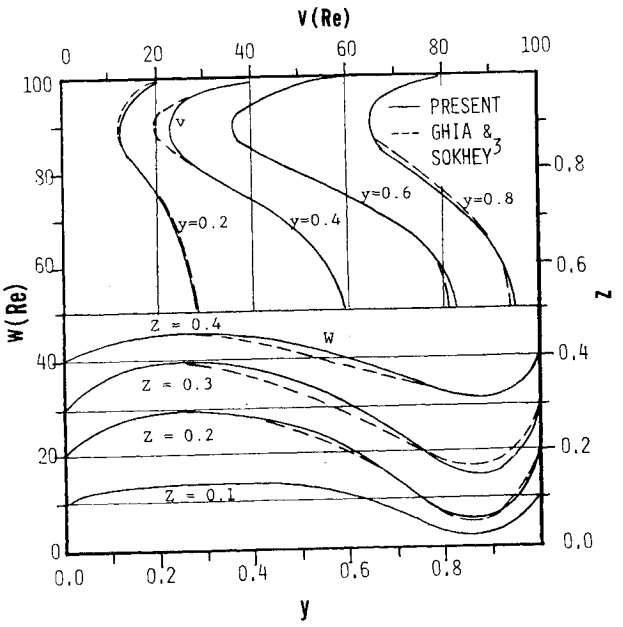

Fig. 5 Fully developed secondary velocity profiles at $\theta = 103$ deg.

Figures 6a-6c show the streamwise development of secondary vorticity and the secondary velocity vectors in the cross section at $\theta = 6.5$, 16.6, and 103 deg, respectively. The vorticity was computed from the nondimensional equation;

$$\omega = \frac{\partial w}{\partial y} - \frac{\partial v}{\partial z}$$

where w and v are nondimensionalized by u_∞ and y and z are nondimensionalized by D. It can be seen that the secondary velocities are from outer to inner radius near the walls and vice-versa near the midspan. It is also clear from these figures that the secondary flow rolls up to form a secondary vortex with a strong core, which is initially ($\theta = 6.5$ deg) located nearly midway between the inner and outer walls. Once the flow is fully developed, the position of the core remains unchanged. The secondary velocities and vortices are large in view of the large flow turning. No experimental data are available for comparison with the predictions.

The computation was carried out on the Pennsylvania State University IBM 3081/370 processor. The run time per marching step is of the order 2.0 s on a 21×21 grid in the cross plane. The run time included I/O time used for disk I/O operations.

Swept Wing[16,17]

The second case computed was a three-dimensional turbulent flow over an infinite wing measured by van den Berg and Elsenaar.[16] The turbulent quantities for the same configuration were measured by Elsenaar and Boelsma.[17] The wing had a swept angle of 35 deg and a chord length of 1420 mm. The flow Reynolds number was 3.4×10^6. The flow developed under a rapid pressure gradient. A diverging channel shape was used to increase the pressure in the flow direction. The flow in front of the diverging channel was maintained parallel to obtain a constant pressure along the forwardmost part of the wing. The spanwise pressure gradient was negligibly small. The three-dimensionality was introduced by the sweep and the chordwise pressure gradient. The coordinate system is shown in Fig. 7. As in the case of a turning duct, the computation was carried out at a Mach number of 0.169. The computation was not affected when the Mach number was increased to 0.25. The number of streamwise steps was 300, and mesh size in the cross-flow plane was 42×5.

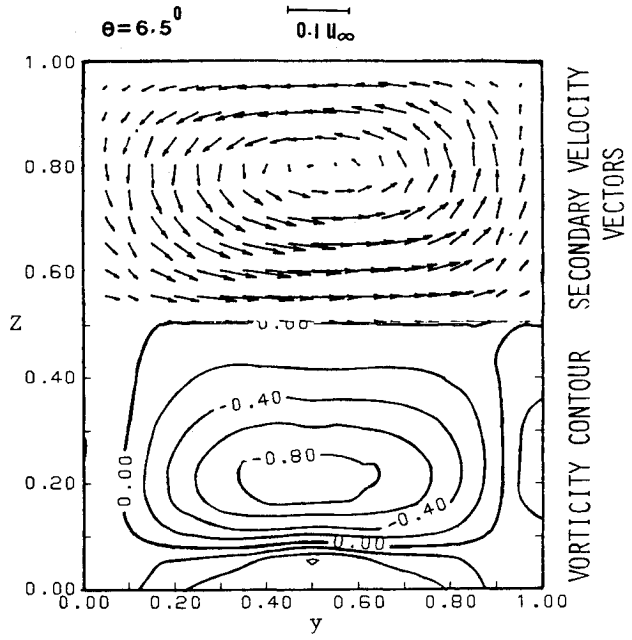

Fig. 6a Secondary vorticity and secondary velocity vectors at $\theta = 6.5$ deg.

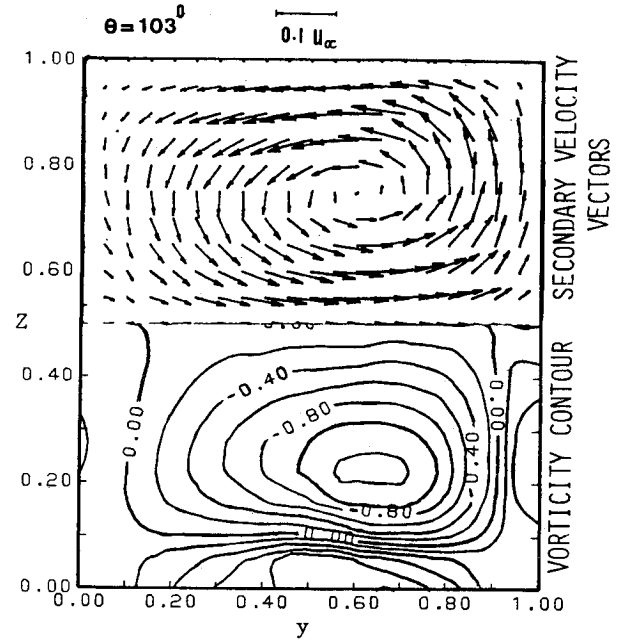

Fig. 6c Secondary vorticity and secondary velocity vector at $\theta = 103$ deg.

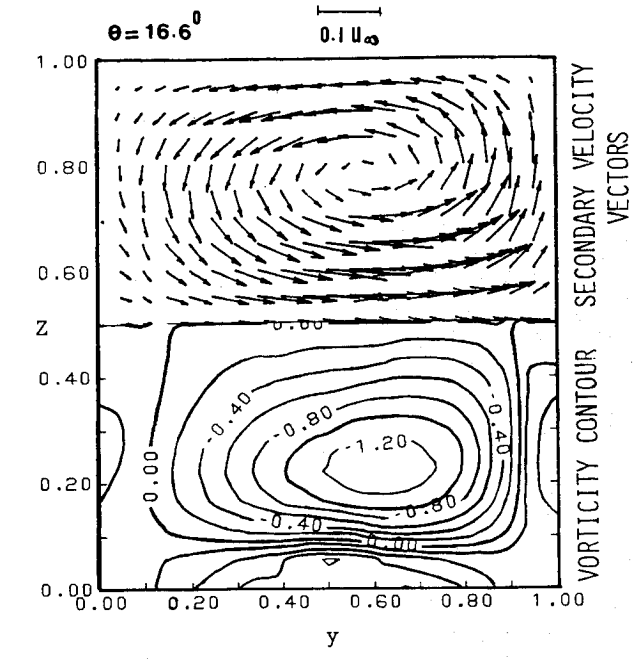

Fig. 6b Secondary vorticity and secondary velocity vectors at $\theta = 16.6$ deg.

The flowfield was computed using both the eddy viscosity and the k-ϵ models. Experimental data at $x'/c = 0.3662$ were used as an initial condition. x' is the distance along the chordwise direction, as shown in Fig. 7. Figures 8 and 9 show the comparison of the experimental and numerical results at $x'/c = 0.7183$. It should be noted that the results presented in Figs. 8 and 9 are in the boundary-layer coordinate system (Fig. 7). The u velocity component, along the freestream direction x, computed from both the models, is in good agreement with the experiment. In these plots, z is the coordinate normal to the wall, δ is the boundary-layer thickness, and u_e is the velocity at the boundary-layer edge. However, the v velocity component in the transverse direction shows significant departure from the experiment, especially near the wall region. The departure might be attributed to insufficient resolution in the region close to the wing surface or inaccuracy in the experimental data, or both. It should be noted that the prediction using the k-ϵ model is good from $z/\delta = 0.3$ to the boundary-layer edge.

The u component of the boundary profiles is plotted in Fig. 10 for various chordwise locations. The results from both the turbulence models are compared with the experimental data. The agreement between the computed results using both models is good up to $x'/c = 0.648$. The results from the algebraic eddy viscosity are better at $x'/c = 0.7183$ and 0.7887 and are identical to the measured data. The prediction using the k-ϵ model is identical to the measured data at $x'/c = 0.8592$. The discrepancy near the wall at other locations ($x'/c \leq 0.649$) may have been caused by insufficient resolution (sparse grid) of the boundary layer or the inaccuracy of the wall functions used in the k-ϵ models. A wall function was used in the k-ϵ model to estimate the values of k and ϵ at the first grid point away from the wall.

The cross-flow velocity profiles (v) at various chordwise locations are shown in Fig. 11. The predictions are good up to $x'/c = 0.6479$, beyond which predictions in the inner region are not good. The discrepancy here may have been caused by the inaccuracy of the computation in the wall region, mentioned earlier, as well as the use of isotropic eddy viscosity models in the computation. As the cross flow gets larger, the effect of anisotropy on eddy viscosity gets larger.

No predictions are shown for $x'/c > 0.8592$, as the flow has separated in these regions. The elliptic effects induced by such separation cannot be resolved by a single-sweep parabolic method used in this paper.

The variation of the turbulent kinetic energy in the boundary layer at $x'/c = 0.7711$ (Ref. 17) is shown in Fig. 12. The computed turbulent kinetic energy is in good agreement with the experiment. This suggests that the turbulent velocity scales were computed accurately. The dissipation rate, which is dictated by the length scale, may be very sensitive to the boundary conditions employed on the no-slip boundary.

The variations of the total shear stress (τ) in the boundary layer at $x'/c = 0.7711$ are shown in Fig. 13. Total shear stress computed using the eddy viscosity model is in good agreement with the experimental data up to $z = 0.2$. The shear stress is overpredicted in the region $z = 0.2$ to 0.8. One reason for this might be the method of computing the eddy viscosity in the

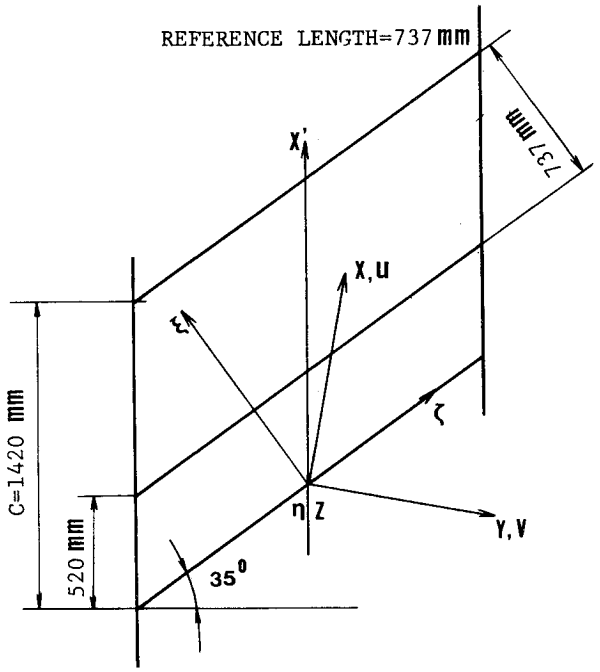

Fig. 7 Swept-wing geometry and coordinate system.

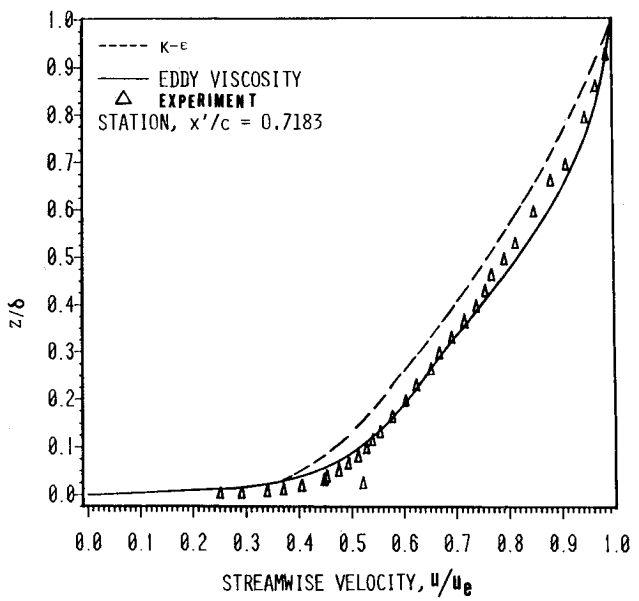

Fig. 8 Comparison of streamwise velocity at $x'/c = 0.7183$.

outer region. The eddy viscosity model of Baldwin and and Lomax[11] avoids the need for locating the boundary-layer edge, and this removes the arbitrariness in the computation. A consequence of this is that the eddy viscosity is slightly overpredicted in the outer region. The computed shear stress using the k-ϵ model is less than the measured values up to $z = 0.35$. In the region $z = 0.3$ to 0.8, the prediction is close to the experimental result. This again suggests that the k-ϵ model is very sensitive to the boundary conditions used in evaluating k-ϵ. Most of the discrepancy between the measured values and the predicted values (using k-ϵ models) occurs near the wing surface.

The computation was carried out on the Pennsylvania State University IBM 3081/370 processor. The run time per marching step was of the order 1.04 s using the k-ϵ model and 0.81 s using the eddy viscosity model on a 42×5 mesh.

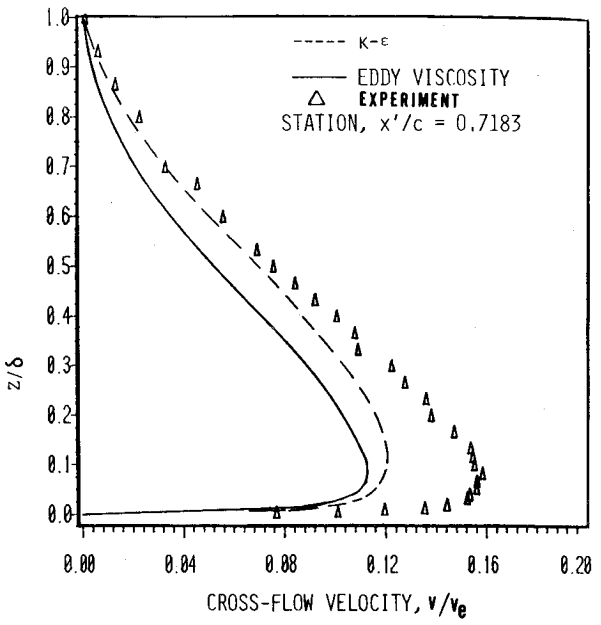

Fig. 9 Comparison of cross-flow velocity at $x'/c = 0.8183$.

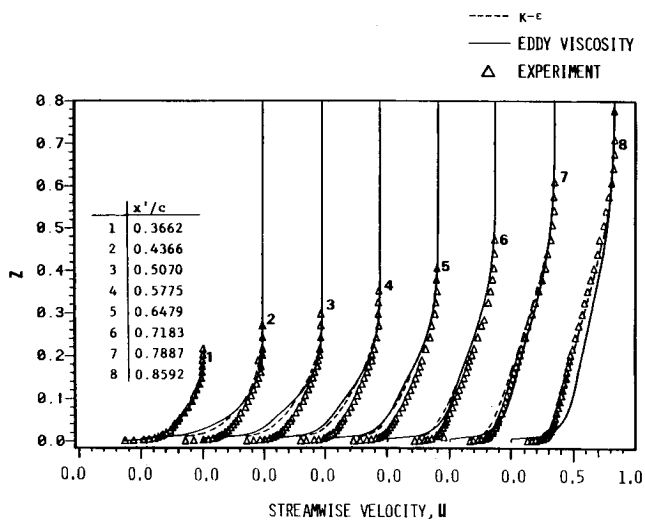

Fig. 10 Development of streamwise velocity profile.

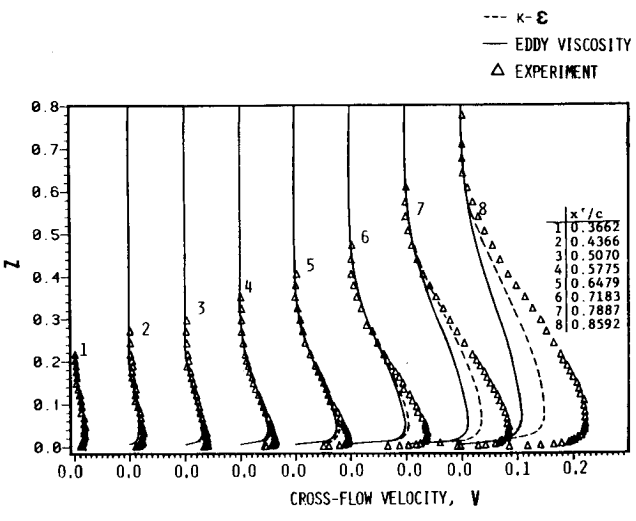

Fig. 11 Development of cross-flow velocity profile.

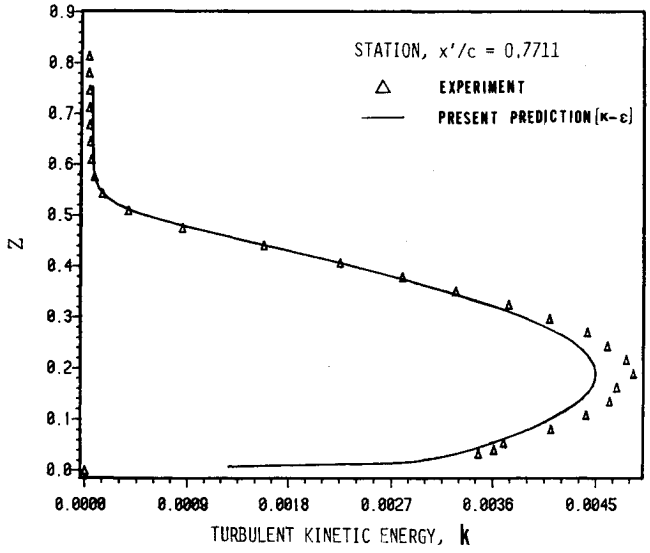

Fig. 12 Prediction of turbulent kinetic energy using k-ϵ model at $x'/c = 0.7711$.

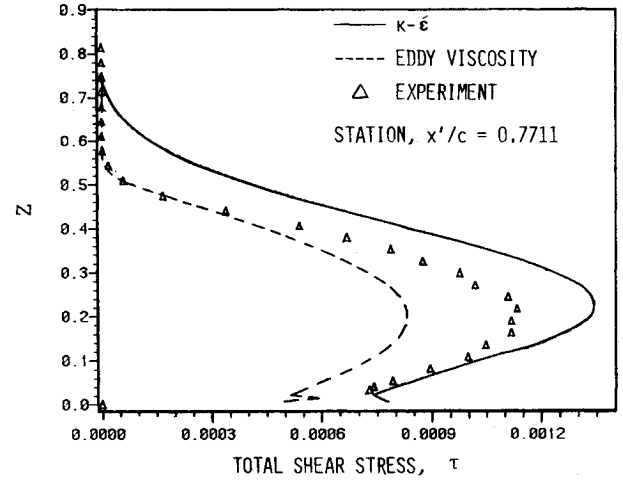

Fig. 13 Prediction of total shear stress using k-ϵ model and eddy viscosity models at $x'/c = 0.7711$.

Concluding Remarks

The present investigation has demonstrated that space-marching methods can be used to predict complex three-dimensional flows, including three-dimensional boundary layer over wings and flow through ducts of large turning. However, a known pressure field which includes most of the elliptic effects is necessary to space-march the solutions. Keeping part of the streamwise pressure implicit helps the march through regions of strong pressure gradients.

In the case of three-dimensional flows, the k-ϵ model was found to be superior to the eddy viscosity model. However, the boundary conditions used in evaluating k and ϵ at the first grid point away from the wing surface affected the computation.

Acknowledgments

This work was supported by the National Aeronautics and Space Administration under Grant NSG 3266 with Dr. P. M. Sockol as the Technical Monitor. The authors wish to acknowledge Dr. T. R. Govindan and Dr. M. Pouagare for their help in this computation.

References

[1]Patankar, S. V. and Spalding, D. B., "A Calculation Procedure for Heat, Mass and Momentum Transfer in Three-dimensional Parabolic Flows," *International Journal of Heat and Mass Transfer*, Vol. 15, 1972, pp. 1787-1806.

[2]Briley, W. R., "Numerical Method for Predicting Three-Dimensional Flow Through Ducts," *Journal of Computational Physics*, Vol. 16, 1974, p. 8.

[3]Ghia, K. N. and Sokhey, J. S., "Laminar Incompressible Viscous Flows in Curved Ducts of Rectangular Cross Sections," *Journal of Fluids Engineering*, Vol. 99, Dec. 1977, p. 640.

[4]Moore, J. and Moore, J. G., "A Calculation Procedure for Three-dimensional, Viscous, Compressible Duct Flow, Parts I and II," *Journal of Fluids Engineering*, Vol. 101, Dec. 1979, p. 415.

[5]Govindan, T. R., "A Space-Marching Method for the Navier Stokes Equations for Internal Flows," Ph.D. Thesis, Dept. of Aerospace Engineering, The Pennsylvania State University, Dec. 1983.

[6]Schiff, L. B. and Steger, J. C., "Numerical Simulation of Steady Supersonic Viscous Flow," *AIAA Journal*, Vol. 18, 1980, p. 1421.

[7]Rakich, J. V., "Iterative PNS Method for Attached Flows with Upstream Influence," AIAA Paper 83-1955, June 1983.

[8]Pouagare, M. and Lakshminarayana, B., "Computation of Viscous Flow in Turbomachinery Cascades," *Computation of Internal Flows: Method and Applications*, American Society of Mechanical Engineers, Fed. Vol. 14, Feb. 1984.

[9]Briley, W. R. and McDonald, H., "On the Structure and Use of Linearized Block Implicity Scheme," *Journal of Computational Physics*, Vol. 34, 1980, pp. 54-73.

[10]Beam, R. M. and Warming, R. F., "An Implicit Factored Scheme for the Compressible Navier-Stokes Equations," *AIAA Journal*, Vol. 16, 1978, p. 393.

[11]Baldwin, B. S. and Lomax, H., "Thin Layer Approximation and Algebraic Model for Separated Turbulent Flows," AIAA Paper 78-257, Jan. 1978.

[12]Jones, W. P. and Launder, B. E., "The Calculation of Low Reynolds Number Phenomena with a Two Equation Model of Turbulence," *Journal of Heat and Mass Transfer*, Vol. 16, 1973, p. 1119.

[13]Gorski, J., Govindan, T. R., and Lakshminarayana, B., "Computation of Three-dimensional Turbulent Shear flows in Corners," AIAA Paper 83-1733, June 1983, *AIAA Journal* (to be published).

[14]Mori, Y., Uchida, T., and Ukon, T., "Forced Convective Heat Transfer in Curved Channel of Square Cross Section," *International Journal of Heat and Mass Transfer*, Vol. 14, 1971, pp. 1787-1805.

[15]Cheng, K. C., Lin, R., and Ou, J., "Fully Developed Laminar Flow in Curved Rectangular Channels," ASME Paper No. 75-FE-4, May 1975.

[16]van den Berg, B., and Elsenaar, A., "Measurement in a Three-dimensional Incompressible Turbulent Boundary Layer in an Adverse Pressure Gradient Under Infinite Swept Wing Condition," National Aerospace Laboratory, The Netherlands, TR 72092U 1972. (See also *Journal of Fluid Mechanics*, Vol. 70, 1975, p. 127.)

[17]Elsenaar, A. and Boelsma, S. H., "Measurement of the Reynolds Stress Tensor in a Three-dimensional Turbulent Boundary Layer Under Infinite Swept Wing Conditions," National Aerospace Laboratory, The Netherlands TR 74095U, 1974.